Journal of Materials Chemistry B

Accepted Manuscript

ROYAL SOCIETY OF CHEMISTRY

www.rsc.org/materialsB

Journal Name

ARTICLE

Laser light triggered smart release of Silibinin from a PEGylated-PLGA gold nanocomposite

Received 00th January 20xx,
Accepted 00th January 20xx

DOI: 10.1039/x0xx00000x

www.rsc.org/

E. Fazio,*[a] A. Scala,*[b] S. Grimato,[a] A. Ridolfo,[a] G. Grassi[b] and F. Neri[a]

In this work a new remotely-triggered drug delivery system based on PEG-PLGA_Au nanocomposite is proposed. Due to the optical properties of gold nanoparticles (Au NPs), the nanovector allows on-demand control of the dose, the timing and the duration of the drug release, upon irradiation with red laser light. The Au NPs are synthesized by laser ablation and subsequently embedded into the PEG-PLGA copolymer *via* a modified emulsion-diffusion method, devised in such a way that both Au NPs and Silibinin (SLB), a flavonolignan with promising anti-neoplastic effects, can be co-loaded into the polymeric system in a single step procedure. A combination of analytical techniques including Nuclear Magnetic Resonance (NMR), Static and Dynamic Light Scattering (SLS, DLS), Gel Permeation Chromatography (GPC), Thermogravimetric Analysis (TGA), X-Ray photoelectron (XPS), Infrared (FTIR) spectroscopies, Scanning/Transmission Electron Microscopies (SEM/STEM/TEM), has been used to study the structural and morphological properties of the nanocomposite. The loading efficiency and the drug content, evaluated by UV-vis absorption optical spectroscopy, are 89% and 8.8%, respectively. Upon laser irradiation the system releases the encapsulated drug with a higher efficiency (~10%) than that not irradiated. This behaviour indicates that our nanoplatform is responsive to light and it could be considered a promising new type of light-activated drug delivery carrier applicable to the biomedical field.

Introduction

Stimuli-responsive drug delivery systems (DDSs) are mainly designed to respond to internal and/or external triggers, providing the drug concentration within its therapeutic window to target site upon a specific stimulus. Nanoparticles-based drug carriers are very appealing as they could be triggered by a variety of stimuli, such as temperature, pH, light, magnetic field, enzymes, releasing drugs to a desirable site of action, at accurate timing or conditions.[1,2]

In this view, Au NPs are valuable building blocks for the development of DDSs, because they exhibit low cytotoxicity and good cell permeability. Due to their high surface to volume ratio and easy interaction with biomolecules (e.g. enzymes, antibodies, DNA) and cells, they are very attractive candidates for use as carriers in medical diagnosis and treatment,[3] and for a wide variety of biomedical applications (biological sensing, imaging and nanomedicine) derived from their optical properties.[4] In fact, they are well known for their Surface Plasmon Resonance band (SPR), a phenomenon associated with coherent oscillations of conduction-band electrons on NPs surface upon interaction with light.[5] As Au NPs can interact with external light,[6] gold nanostructure-containing capsules afford a promising light responsive drug carrier. To date, the light-triggered release of encapsulated molecules from Au NPs-embedded liposomes,[7] or polyelectrolytes,[8] mesoporous silica-coated gold nanorods,[9] and gold nanoshell–hydrogel conjugates[10] have been reported.

In addition, Au NPs can efficiently convert the absorbed energy into heat which might be used for hyperthermal cancer therapy or photothermal drug delivery.[4]

Various methods have been reported over the last two decades for the synthesis of Au NPs, which involved the reduction of $AuCl_4^-$ with a chemical reducing agent, such as citrate, borohydride, or other organic compounds.[11] In the case of sodium citrate reduction, the citrate acts as a loosely bound capping agent stabilizing the particles. Tetradecane, octadecane or dodecane thiols are often used as capping agents to stabilize AuNPs produced via sodium borohydride reduction.[12] Furthermore, biological responses can be altered using capping agents such as polyethylene glycol,[12-13] mercaptosuccinic acid, various proteins or other biomolecules.[14]

Additionally, Au NPs can be synthesized by laser ablation, using a pulsed laser beam to ablate a metal target immersed in a solvent. Such a technique offers several advantages: the production of NPs may occur in a variety of solvents, no surfactant is needed to stabilize the colloid, the NPs can be extremely pure and, finally, a fine-tuning of the process allows the production of NPs which can differ in size and properties.[15]

[a] Dipartimento di Scienze Matematiche e Informatiche, Scienze Fisiche e Scienze della Terra, Università di Messina, V.le F. Stagno d'Alcontres 31, 98166, Messina, Italia. E-mail: enfazio@unime.it
[b] Dipartimento di Scienze Chimiche, Biologiche, Farmaceutiche ed Ambientali, Università di Messina, V.le F. Stagno d'Alcontres 31, 98166, Messina, Italia. E-mail: ascala@unime.it

† Footnotes relating to the title and/or authors should appear here.
Electronic Supplementary Information (ESI) available

The stability of the gold nanocolloids are maintained by the negative charges on the NPs surface. Au NPs generated by pulsed laser ablation are naturally negatively charged, being partially oxidized by the oxygen present in water. Therefore, additional chemical agents are not required to stabilize these chemically pure Au NPs against aggregation.[16] On the other hand, when Au NPs are included within a polymeric matrix, the obtained nanocomposite approachs a positive zeta potential value, indicating that the mechanism of stabilizing laser-generated colloidal Au NPs is changed from electrostatic repulsion to steric repulsion (Steric shielding effect) with PEG, stabilizing the nanosuspensions for its successful long-term storage.[17]

Among the numerous studied drug delivery systems, polymeric NPs are considered particularly interesting colloidal systems in which the therapeutic agent is dissolved, entrapped, encapsulated, or adsorbed onto the constituent polymer matrix.[18] Furthermore, polymeric nanostructures bearing a hydrophobic inner core and hydrophilic outer shell have received great attention due to their excellent properties in drug delivery.[19,20] They are considered ideal vehicles for antitumor drug delivery due to their ability to self-assemble into spherical nanosized core/shell structure in aqueous media forming polymeric micelles.[18] In particular, their hydrophobic inner core is an appropriate reservoir for hydrophobic anticancer drugs and their hydrophilic outer shell facilitates avoidance of the reticuloendothelial system, long blood circulation, and the improvement of enhanced permeation and retention (EPR) effect in tumor tissue.[21]

Various aliphatic polyesters approved by the US Food and Drug Administration (FDA), such as poly(L-lactic acid) (PLA), poly(DL-lactic-co-glycolic acid) (PLGA), and poly(e-caprolactone) (PCL), have been combined with a hydrophilic PEG segment to produce amphiphilic copolymer structures.[22] Among them, PEGylated poly(lactic-co-glycolic acid) (PEG-PLGA) nanocomposites are considered interesting hybrid systems due to their hydrophobic and hydrophilic properties, forming core-shell type nanostructures. In addition, they are biodegradable, non-toxic, and non-immunogenic.[23] Particularly, PEG conjugation to PLGA offers various beneficial outcomes, such as: (a) increase of the aqueous solubility and stability, (b) reduction of intermolecular aggregation, (c) increment of the systemic circulation time, (d) preparation of self assembling micelles. In addition, the end groups of PEG can be derivatized and/or conjugated with ligands for passive and ligand-targeted delivery of therapeutics.[18] In this case, targeting agents, such as folate, transferrin, epidermal growth factor receptors (EGFRs) and glycoproteins can be grafted at the NPs surface via a linkage on PEG chains to bind specific receptors over-expressed by tumor cells, enhancing cellular uptake of NPs through endocytosis.[24]

Recently, a wide variety of drug formulations such as micro/nano-particles, micelles, hydrogels, injectable systems have been developed with PEG-PLGA copolymers[25] and used as tissue engineering scaffold,[26] and delivery systems[18,27-30] for both hydrophilic and hydrophobic small drugs (doxorubicine, paclitaxel),[31-35] vaccines and biomacromolecules.[36]

To date, only four targeted polymeric NPs have progressed in clinical development,[37] one of which is BIND-014, a docetaxel formulation that recently entered Phase II clinical testing for the treatment of patients with solid tumors, developed by a team led by Langer and Farokhzad at the Massachusetts Institute of Technology, Harvard Medical School, and BIND Therapeutics. BIND-014 comprises a biodegradable copolymeric core (PLA and PEG), a pseudo-mimetic dipeptide as a PSMA-targeting ligand, and docetaxel as the anticancer drug.[37,38]

Generally, drugs entrapped into polymeric NPs are primarily released in a passive manner, usually by simple diffusion during spontaneous hydrolysis of the polymer matrix. This is normally a slow process that may take a few days to months.[39,40] Otherwise, active release of drug in a controllable manner may be provided by incorporating thermal activated Au NPs in the polymer matrix, following laser light irradiation. The localized and intensive heating of Au NPs results in a thermal expansion of the polymer, thus the drug starts to diffuse out. With such a design, the loaded drug molecules can be triggered to be released in an active and controllable manner.[41-45] Recently, a few papers reported about the preparation of AuNPs/polyester composites[46,47] for the controlled release of anticancer and antitubercolosis drugs, such as metotrexate,[48] docetaxel[49] and rifampicin.[50]

In the present study, for the first time, Au NPs synthesized by laser ablation were embedded into the PEG-PLGA copolymer previously prepared, *via* a modified emulsion-diffusion method devised in such a way that both Au NPs and drug can be co-loaded into the polymeric system in a single step procedure. To check for the controlled laser light triggered release of incorporated drug, Silibinin (SLB), a polyphenolic flavonoid, has been successfully loaded into the nanovector. Fig.1 illustrates the strategy for preparation of our SLB-loaded PEG-PLGA_Au nanosystem.

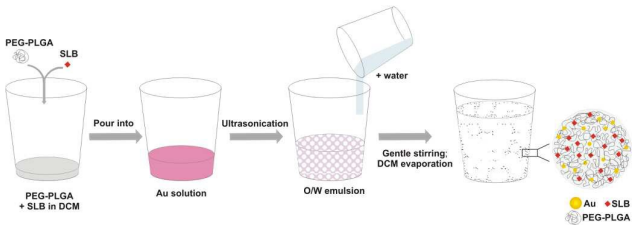

Fig. 1: Schematic illustration of the synthesis of our PEG-PLGA_Au-SLB nanocomposite.

SLB, a flavonoid compound extracted from the fruit of *Silybum marianum*, a plant of Asteraceae, is reported to possess multiple biological activities and it is currently in phase II clinical trials in patients with prostate cancer.[51] However, its use in the preparation of pharmaceutical products is limited by its low solubility which greatly reduces the oral bioavailability. Nanoparticles-based DDSs have emerged as a new tool to overcome these issues. To date, only a few reports describe the preparation of SLB-loaded formulations, such as

nanosuspension,[52] nano-structured lipid carriers,[53-55] hydrogel,[56] and self-emulsifying drug delivery system.[57]

To the best of our knowledge, this is the first paper reporting the effects of laser light irradiation (632.8 nm) on the release efficiency of SLB from a PEG-PLGA_Au nanoplatform.

In this work the compositional/structural features of both SLB-loaded and unloaded nanocomposites have been fully investigated using a combination of analytical techniques including NMR, GPC, SLS, TGA, FTIR and XPS spectroscopies. The morphology has been characterized by SEM/STEM/TEM microscopies and Dynamic Light Scattering (DLS) measurements. The drug loading and the drug release profile were determined by UV-Vis optical absorption spectroscopy. In particular, the release of SLB was studied both upon and without laser light irradiation, with the aim to compare the rate and the efficiency of released drug.

2. Experimental

2.1. Materials

Poly(lactic-co-glycolic acid) (PLGA, molar ratio of D,L-lactic to glycolic acid, 50:50, MW= 24-38 kDa), poly(ethylene glycol) (PEG, MW=8 kDa), stannous 2-ethylhexanoate, dichloromethane (DCM), anhydrous toluene (purity 99,8%), and SLB were purchased from Sigma-Aldrich; the high purity (99.99%) gold target from Mateck srl.

2.2. Characterization techniques

^{1}H-NMR and ^{13}C-NMR spectra were recorded at room temperature using a Varian 500 MHz spectrometer. Chemical shifts (δ) were expressed in ppm using tetramethylsilane (TMS) as an internal reference.

The Fourier Transform Infrared (FTIR) spectra were collected in the 4000-600 cm^{-1} range, using the Spectrum 100 Perkin-Elmer spectrometer in ATR configuration.

XPS spectra were acquired using a K-Alpha system of Thermo Scientific, equipped with a monochromatic Al-Kα source (1486.6 eV) and operating in constant analyser energy (CAE) mode with a pass energy of 20 eV for high resolution spectra and a spot size of 400 µm. The analysis procedure was performed with the Avantage software of K-Alpha system and every core level photoemission peak was deconvoluted with Gauss–Lorentzian shape functions with the same FWHM (1.4) for all the considered subbands.

SEM analyses were carried out with the Zeiss-Gemini 2 electron microscope, operating at 30 kV and at a working distance of 4 mm when the measure was carried out in transmission mode (STEM) and at an accelerating voltage of 150 KV for the collection of the SEM images. SEM apparatus is coupled with a Quantax EDX spectrometer to carry out Energy Dispersive X-ray (EDX) analysis. The EDX detected pear-shaped dimension is about 0.7 µm. Samples were dispersed in PBS/DMSO (1:99) using the Sonics VCX 130 ultrasonic sonicator; then a drop of each suspension was deposited, respectively, on a 400 mesh holey-carbon grid and left to dry at room temperature for 3h or a carbon support sputter-coated with chromium.

Transmission Electron Microscopy (TEM) measurements were carried out with a JEOL JEM 2010 electron microscope (LaB 6 electron gun) operating at 200 kV, equipped by a Gatan 794 Multi-Scan CCD camera for digital imaging. Samples for TEM analysis were prepared by dropping a suspension of the sonicated samples on a 400 mesh holey-carbon coated copper grids.

Dynamic Light Scattering (DLS) measurements were performed using an Horiba NanoParticle Analyzer SZ-100 (range: 0.3 nm - 8 µm). Using the same Horiba NanoParticle Analyzer SZ-100, the Zeta potential was quantified with a laser Doppler method, based on the principle of electrophoretic mobility under an electric field.

UV–vis absorption spectra were collected by means of a Perkin-Elmer Lambda 750 UV-vis spectrometer in the range 190-1100 nm using quartz cells.

GPC measurements were performed using the Agilent GPC-Addon system and a RID-A refractive index signal detector coupled to the PLgel columns. Tetrahydrofuran and DMSO were used as an eluent (flow 1ml/min) and the sample injection volume was 10 µl.

Thermal degradation of the investigated copolymers was monitored by TGA using a Mettler Toledo TGA 851 apparatus (horizontal balance mechanism) in air. Each sample was placed in an open alumina crucible. The sample weight is 5 mg. The thermogravimetric weight loss curve was recorded as a function of temperature. Firstly, the samples were kept at 25°C under a 10 ml/min air flow until balance stabilization, then heated at the maximum programmed heating rate (nominally 1000°C/min). The constant heating rate of 10°C/min was employed. Balance sensitivity was 0.5 µgr. The weight loss was calculated through the difference between the weights at rt and at 900°C.

2.3. Synthesis and purification of PEG-PLGA copolymer

PLGA (500 mg, 1 equiv) and PEG (258 mg, 2 equiv) were dissolved in 20 mL anhydrous toluene in a two-necked flask equipped with a stirrer, water-cooled condenser, and argon inlet. Stannous 2-ethylhexanoate (0,22 equiv) was added to the solution as catalyst. The flask was heated at 105 °C for 18 h. Then, the solvent was evaporated under reduced pressure. The residue was dissolved in DCM (13 ml), then the solution was added to vigorously stirred water (65 ml) at 60 °C for 1h. After DCM evaporation from the emulsion, a solid was isolated from the aqueous phase by centrifugation at 6000 rpm for 20 min (ALC Refrigerated Centrifuge PK120R) and washed twice with water.

2.4. Au NPs synthesis

The 532 nm second harmonic emission wavelength of a Nd:YAG laser, operating at a repetition rate of 10 Hz (pulse length: 5 ns), was used to prepare the Au water colloids. The beam was focused on the surface of the gold target (3 mm thickness, 99.99% purity) through a mirror tilted at 45° and a lens with 20 cm of focal length. The laser spot size was about

2 mm in diameter. The ablation process was carried out using a laser fluence of 1.5 J/cm^2, 20 mm of water above the target and an ablation time of 20 min. After preparation, all the solutions were stirred at room temperature in an ultrasonic bath for about 15 min and immediately assembled with the PEG-PLGA copolymer.

2.5. Preparation of PEG-PLGA_Au nanocomposite

50 mg of PEG-PLGA copolymer were dissolved in 1 ml of DCM at room temperature, rapidly poured into 9 ml of freshly prepared gold solution at rt and emulsified by ultrasonication for 10 min (Sonics VCX 130). The addition of a large volume of aqueous solution (4 times the volume of the emulsion) to the oil-in-water emulsion (O/W) under gentle stirring, at rt for 1 hour, induces solvent diffusion into the external phase. A solid was isolated from the aqueous phase by centrifugation at 6000 rpm for 20 min. This workup procedure allows to eliminate the low molecular weight copolymer fraction.

2.6. Preparation of SLB-loaded PEG-PLGA_Au nanocomposite

SLB-loaded PEG-PLGA_Au nanocomposite at a polymer/drug weight ratio of 50:5 was prepared as follow: PEG-PLGA copolymer (50 mg) and SLB (5mg) were co-dissolved in 1 ml of DCM at room temperature. This organic phase was rapidly poured into 9 ml of freshly prepared gold solution at rt and emulsified by ultrasonication for 10 min (Sonics VCX 130). The addition of a large volume of aqueous solution (4 times the volume of the emulsion) to the oil-in-water emulsion (O/W) under gentle stirring at rt for 1 hour allowed the organic solvent to leave the droplets. A solid was isolated from the aqueous phase by centrifugation at 6000 rpm for 20 min. This workup procedure allows to eliminate the low molecular weight copolymer fraction.

2.7. Drug loading and release

To evaluate the drug content and the loading efficiency, a weighted amount (1 mg) of the nanocomposite incorporating SLB was dissolved in 4 mL PBS, sonicated for 30 min, centrifuged at 6000 rpm for 45 min and repeatedly filtered with a 0.22 μm membrane filter, until free, unbound drug was no more detected. The precipitates were collected, lyophilized, re-dispersed in DMSO/PBS (1:99) and UV–vis spectra were recorded. The SLB amount in the nanocomposite was determined spectrophotometrically, following the absorbance signal at the wavelength (λ_{max}) of 286 nm. The following equations were used to calculate drug content and drug loading efficiency:

-Drug content (%)= (Drug weight in the NPs/Weight of the NPs) x 100.

-Drug loading Efficiency (%)= (Drug weight in the NPs/Weight of drug used in the formulation) x 100.

The in vitro release experiments were performed in 10 mM PBS at pH 7.4 by a dialysis method. Briefly, 4 mg of SLB loaded PEG-PLGA_Au were dispersed in 4 mL of PBS, sonicated for 1 h, and placed in a dialysis bag (MWCO=3.5-5 kD, Spectra/Por®). The sample was plunged in PBS (external bag: 15mL) under stirring and kept at 37 °C. At fixed times, 1 mL of release medium was withdrawn and replaced with an equal volume of fresh one and, then, analyzed by UV-Vis spectroscopy, using the SLB molar extinction coefficient (ε_{286}), previously calculated. The experiment was carried out in duplicate. For the laser light triggered release experiments, a Melles-Griot He-Ne (632.8 nm) continuous laser source was used, with an energy density of 21 mW/cm^2.

3. Results and discussion

3.1. Preparation and characterization of SLB-loaded PEG-PLGA_Au nanocomposite

The SLB-incorporated PEG-PLGA_Au nanocomposite was prepared by a modified emulsion-diffusion method, devised in such a way that both Au NPs and drug were advantageously co-loaded into the polymeric system in a single step procedure (see Experimental).

The ^{1}H NMR spectrum of PEG-PLGA in $CDCl_3$ (see Fig. S1, SI) is consistent with the structure of the copolymer, confirming its successful synthesis. In particular, multiplets at 5.2 ppm and 4.8 ppm are attributed to the methine and methylene groups of the PLGA, respectively; the singlet at 3.64 ppm is assigned to the methylene group of the PEG and overlapping doublets at 1.5 ppm are attributed to the methyl group of the PLGA units.

Since amphiphilic co-polymers, such as PEG-PLGA, are able to form core-shell type NPs in an aqueous environment through a self-assembling process, ^{1}H NMR measurements were further employed both to investigate the core-shell structure of NPs in D_2O and to confirm the drug incorporation (Fig. 2). In particular, as PEG is the hydrophilic domain and PLGA is the hydrophobic domain, our PEG-PLGA nanocomposite has amphiphilic properties and would be able to self-assemble in water as a core-shell type NPs. As expected, the characteristic peak of PEG was the only detected in D_2O, while PLGA and SLB peaks disappeared, indicating that the PLGA-based hydrophobic core is responsible for drug incorporation while the water-soluble PEG backbone constitutes the outer shell. However, all the peaks of PEG, PLGA and SLB are visible in DMSO-d_6, solvent in which the system is disassembled, according to literature.[58,59]

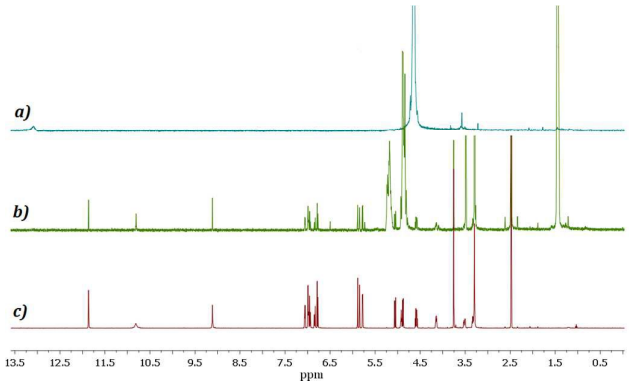

Fig. 2 ^{1}H-NMR of SLB-loaded PEG-PLGA_Au in D_2O (a); SLB-loaded PEG-PLGA_Au in DMSO-d_6 (b); free SLB in DMSO-d_6 (c).

Furthermore, NMR signals are good and clear indications for distinguishing the block and random copolymers.[60] In the ^{13}C NMR spectrum of PEG-PLGA copolymer (see Fig. S2A,SI), the seven major resonances corresponding to the methyl, methylene, methine, and carbonyl groups of PLGA and PEG segments were observed at 16.7 ppm (methyl of PLGA), 60.8 ppm (methylene of PLGA), 69.0 ppm (methine of PLGA), 70.5 ppm (methylene of PEG), 166.3 ppm (carbonyl of PLGA), and 169.3 ppm (carbonyl of PLGA). The expanded ^{13}C NMR spectrum both in the carbonyl and in the aliphatic regions (Fig. S2B and C,SI) shows additional peaks due to the interactions of the different moiety sequences randomly distributed along the copolymer chains, suggesting that our PEG-PLGA is a random copolymer.

Static light scattering (SLS) and gel permeation chromatography (GPC) measurements were carried out to determine the number average molecular weight (M_n), weight average molecular weight (M_w) and polydispersity index (P_d) of PEG-PLGA, PEG-PLGA_Au and PEG-PLGA_Au-SLB (Table 1, Fig. S2,SI, Fig.S3,SI).

Sample	SLS		GPC		
	M_w (KDa)	2nd virial coefficient (A_2)[a]	M_n (KDa)	M_w (KDa)	P_d (M_w/M_n)
PEG-PLGA	38.3	$1.77x10^{-5}$	22.8	39.1	1.71[b]
PEG-PLGA_Au	39.5	$1.80x10^{-5}$	38.5	42.8	1.11
PEG-PLGA_Au-SLB	42.3	$1.93x10^{-5}$	44.1	43.5	0.98

[a]The A_2 positive values indicate that all the nanocomposites tend to stay in solution, avoiding aggregation process.

[b]The low molecular weight copolymer fraction is eliminated in the successive work up procedures (See Experimental).

Table 1: SLS and GPC measurements.

The thermal degradation of the samples was studied by thermogravimetric analysis (TGA) under air flow, pointing out that PEG-PLGA and PEG-PLGA_Au are more stable and starts degradation later than PEG-PLGA_Au-SLB (Fig. S3,SI).

Additionally, the residues of 0.3% and 1.8% of the PEG-PLGA and PEG-PLGA_Au samples respectively, recovered after thermooxidative scannings at 900°C, allow to estimate that the percentage of Au loaded into the nanocomposite is about 1.5%, which is in good agreement with XPS and EDX data (0.7 and 2%, respectively, see below).

The gold content of the nanocomposite was indirectly calculated by analyzing UV–vis optical absorption spectral features and taking into account microscopy results (see Fig. S4, and the procedure adopted to estimate the Au amount in the SI). On the overall, the estimated concentration of the Au colloid in the copolymer is about 1.0 X 10^{-6} M, assuming an average molar extinction coefficient of 2.5 X 10^{4} $M^{-1}cm^{-1}$.

The FTIR spectra of PEG-PLGA and PEG-PLGA_Au have been compared with the standard spectra of free PEG and free PLGA to confirm the successful formation of the new ester linkage of the copolymer (Figure 3). In the IR spectrum of the copolymer PEG-PLGA (black trace), all the PLGA and PEG characteristic peaks are preserved and a shift of the carbonyl stretching frequency is observed from 1753 cm^{-1} for free PLGA (red trace) to 1749 cm^{-1} for PEG-PLGA copolymer (Figure 3c). Moreover, the introduction of gold into the nanocomposite induces: *i)* the disappearance of the band at 2883 cm^{-1}, due to both the -CH_2 and the -CH groups stretching vibrations (Figure 3b); *ii)* slight modifications and shift of bands in the 1400-1200 cm^{-1} spectral range attributed to the vibrational wagging and twisting CH_2 modes (Figure 3d); *iii)* a slight shift of the intense band at 1088 cm^{-1} due to the C-O stretching, indicative of the conjugation of oxygen atoms with the Au NPs (Figure 3d).

The chemical composition of the surface layer (5-10 nm) of PEG-PLGA, PEG-PLGA_Au and PEG-PLGA_Au-SLB was determined by XPS. The C, O, Au species were observed in the surface layer and their percentage (calculated using XPS area and atomic sensitivity factors),[61] were given in relative atomic percentage. From the binary PEG-PLGA to the PEG-PLGA_Au ternary copolymer, the oxygen atomic percentage decreases (from 36.5% down to 30.5%), while the carbon content increases (from 63.5% up to 68.8%), suggesting that some oxygen terminations are surface located and easily bonded to Au NPs (whose amount is 0.7%).

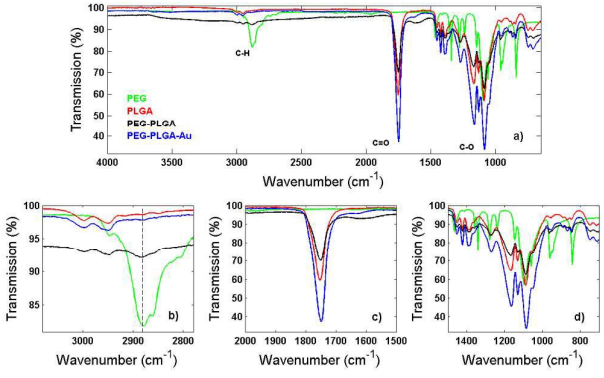

Fig. 3: IR spectra of PEG-PLGA (black trace) and PEG-PLGA_Au composites (blue trace). The IR spectra of PEG and PLGA powders (green and red traces, respectively) are shown for comparison.

The composition of the system was also determined by EDX analysis in different points of the sample. The estimated C (on average 50%), O (on average 45%), and Au (on average 2%), percentages vary slightly from one point to another one of the sample (Table 2), but are still in good agreement with XPS data.

Element	EDX atomic (%) Point 1	EDX atomic (%) Point 2	EDX atomic (%) Point 3	EDX atomic (%) Point 4
C	66.0	73.7	68.7	80.6
O	32.4	25.0	29.7	17.0
Au	1.6	1.3	1.6	2.4

Table 2: Atomic species percentage determined by EDX analysis. Chemical characterization in the scanning electron microscope (SEM) is performed non-destructively with energy dispersive X-ray analysis (EDX). The electron beam stimulates the atoms in the sample with uniform energy and they instantaneously send out X-rays of specific energies for each element, the so called characteristic X-rays. This radiation gives information about the elemental composition of the sample.

The C1s lineshapes of PEG-PLGA, PEG-PLGA_Au and SLB-loaded PEG-PLGA_Au are reported in Fig. 4a. The addition of Au to PEG-PLGA copolymers induces a slight decrease of the carbon-oxygen bond contribution at around 286.5 eV. In the SLB-loaded PEG-PLGA_Au composite, the intensity increase of the contributions at higher binding energies (O=C-C*(-C)-O and O=C-O bonds) shows the presence of the drug within the copolymer.

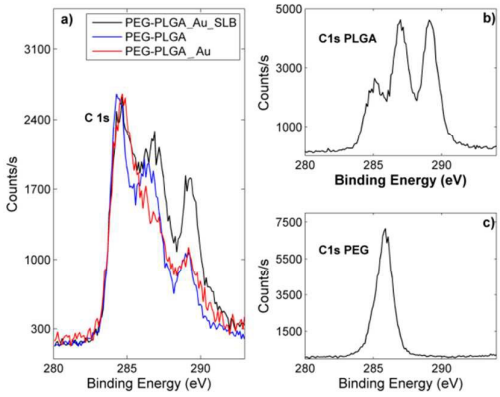

Fig. 4: C1s XPS lineshapes of (a) PEG-PLGA, PEG-PLGA_Au and SLB loaded PEG-PLGA_Au composite; (b) PLGA and (c) PEG powders.

As shown in Fig. 4b there is a difference of 0.8 eV between the binding energies of C-O (namely C-OH contribution) from PEG and C-O from PLGA, which enables an easy distinction of the two polymers. Therefore, C1s profiles have been deconvolved considering five spectral components centred at about 284.5, 285.5, 286.3, 287.0 and 289.2 eV, corresponding to the C-C; C-OH; C-O; O=C-C*(-C)-O and O=C-O bonds, respectively. The contribution at 290 eV is ascribed to π-π bounds. Fig. 5 reports characteristic high-resolution C1s deconvolution spectra of PEG-PLGA and PEG-PLGA_Au samples, while in Table 3 the values of the bonding fractions of carbon and oxygen atoms are reported.

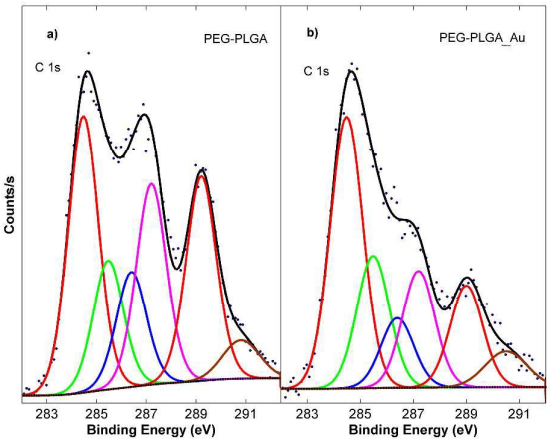

Fig. 5: C 1s deconvoluted profiles.

C1s						
Sample	C-C (%)	C-OH (%)	C-O (%)	O=C-C*(-C-)-O (%)	O-C=O (%)	π–π (%)
PEG-PLGA	28.4	13.3	11.9	20.7	21.0	4.7
PEG-PLGA_Au	36.7	17.9	9.5	15.8	13.9	6.2
PEG-PLGA_Au-SLB	39.2	11.0	21.2	14.6	14.0	0.0

O1s				
Sample	O-C PEG (%)	O=C (%)	O-C PLGA (%)	Adsorbed H_2O (%)
PEG-PLGA	4.7	62.5	29.6	3.2
PEG-PLGA_Au	8.9	58.3	27.5	5.3
PEG-PLGA_Au-SLB	4.3	61.5	29.8	4.4

Table 3: Carbon and oxygen bonding fraction determined by XPS analysis.

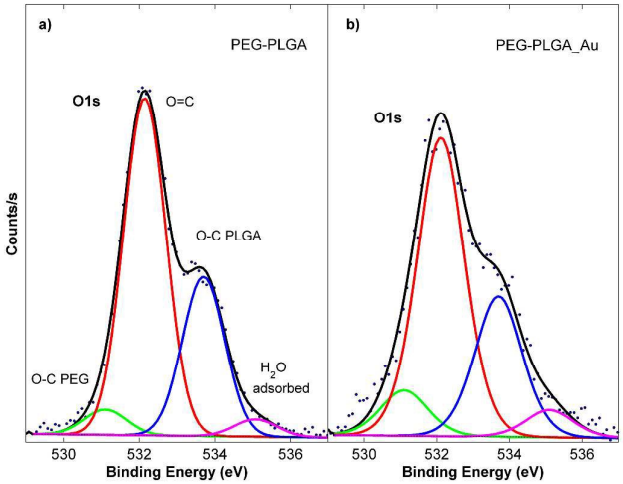

Fig. 6: O1s lineshape of (a) PEG-PLGA and (b) PEG-PLGA_Au.

The results obtained by the C 1s lineshape deconvolution are confirmed by the O 1s fitting results. The O 1s profile of the

copolymers shows four spectral components at 531.1, 532.1, 533.4 and 534.6 eV, corresponding to the PEG O-C bonds, the O=C bonds, the PLGA related O-C bonds and the adsorbed H_2O contribution (Fig. 6a and Table 3). In the presence of Au NPs, the percentage of the PEG O-C bonds increases, while the PLGA related O=C and O-C one decreases. The increased percentage of the C-C and C-OH bonding fractions and mainly the decrease of the C-O, O=C-C*(-C)-O and O=C-O percentages in the PEG-PLGA_Au systems with respect to PEG-PLGA ones (Table 3) are indicative once again of the conjugation of some oxygen terminations with Au NPs.

Particle size and particle distribution width were determined by DLS. DLS measurements show that the PEG-PLGA_Au composite hydrodynamic diameter on an ensemble average is about 90 nm with a PDI value of 0.5 (where 0.5 refers to the most polydisperse population), while the pulsed laser ablated Au NPs are monodispersed with a size of about 20 nm and a PDI value of 0.3.

Some detailed information about the investigated system was obtained by SEM. Fig. 7 shows a SEM image of the PEG-PLGA copolymer, characterized by sponge-like spheres with an average size of 200 nm. The surface of these nanostructures appears bumpy and contains pores (see the inset of Fig. 7). These features can be explained taking into account an interfacial tension instability, dependent on the organization of the polymer at the interface during the emulsion-evaporation process.[62] As long as there is enough dichloromethane to solubilize PEG chains, the copolymer remains in the bulk of the hydrophobic solvent. When the copolymer reaches its solubility limit in dichloromethane, it migrates to the interface to expose PEG moieties towards the aqueous phase. According to literature,[62] in order to expose all the PEG chains to the aqueous environment, some interface must be created, explaining the observed spherical protrusions.

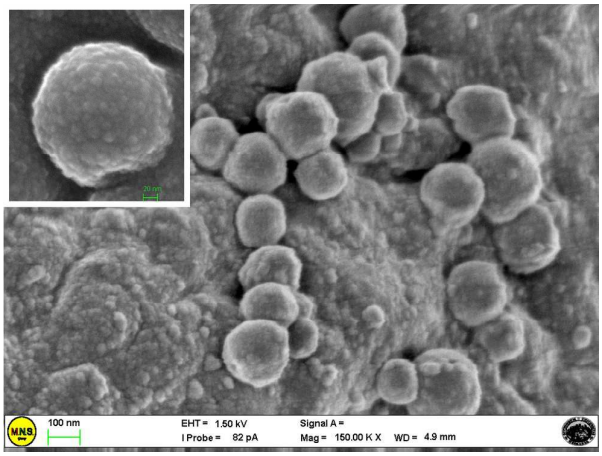

Fig. 7: SEM image of the PEG-PLGA copolymer. In the inset a single 200 nm sized particle.

No relevant differences emerged looking at the SEM images of PEG-PLGA_Au and SLB-loaded composite (data not shown) with respect to the SEM image of PEG-PLGA copolymer shown in Fig. 7. Given to the porous morphology of these samples, Au NPs cannot be distinguishable by SEM images even if they are detected by the EDX probe. For this reason we have carried out SEM measurements in the transmission mode (STEM) and TEM measurements for an higher resolution. The STEM image of the PEG-PLGA_Au-SLB (Fig. 8) shows that Au NPs uniformly decorate the nanocomposite, with a size in the range of 5-50 nm (red circles), in agreement with the hydrodynamic "average" one obtained by DLS and also by the size estimated by TEM (Fig. 9A and Fig. 9B). Particularly, the TEM image of PEG-PLGA_Au nanocomposite consists of not assembled Au NPs, with a measured diameter of about 5-10 nm, randomly distributed throughout the PEG-PLGA copolymer.

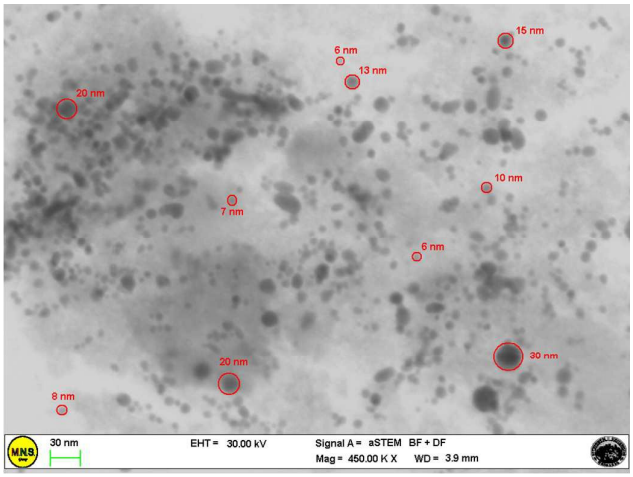

Fig. 8: STEM image of PEG-PLGA_Au-SLB system.

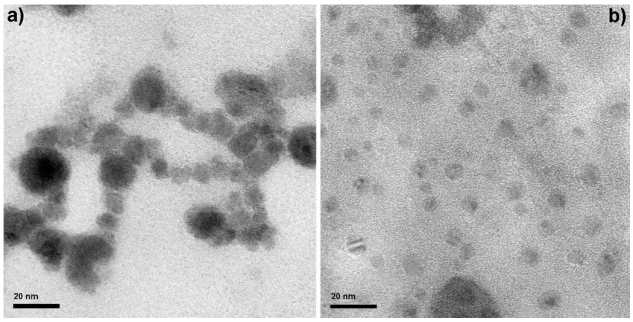

Fig. 9: TEM images of (a) Au NPs prepared by pulsed laser ablation in water and (b) PEG-PLGA_Au nanocomposite.

Furthermore, zeta potential value, which measures the electrostatic potential that exists on the NPs surface, reveals information regarding the surface charge and stability of the nanoparticulate formulation. Au NPs and non coated PLGA polymer show a negative charge (zeta potential value of - 40 mV and -30 mV, respectively; Fig. 10), indicating a relative stability of the colloidal solution, ruling out the possibility of aggregation processes, while the PEG-PLGA_Au nanocomposite shows a much less negative value (- 2.5 mV). The partial shielding of the NPs surface charges is attributed

to the PEG layer formed on the surface, that reduces the electrophoretic mobility and stabilizes the system, for its long-term storage, according to literature.[63] The SLB loaded PEG-PLGA_Au shifts towards a positive zeta potential value of +5.6 mV (Fig. 10), allowing an easy absorption to negatively charged cellular membrane and contributing to a more effective intracellular trafficking.[64] Furthermore, long-term stability of the composites was assessed after freeze-drying at the temperature of 4°C and 25°C by UV-vis absorption measurements. After three months no reduction of the overall optical absorbance is observed, indicating the high stability of the PEG-PLGA_Au NPs.

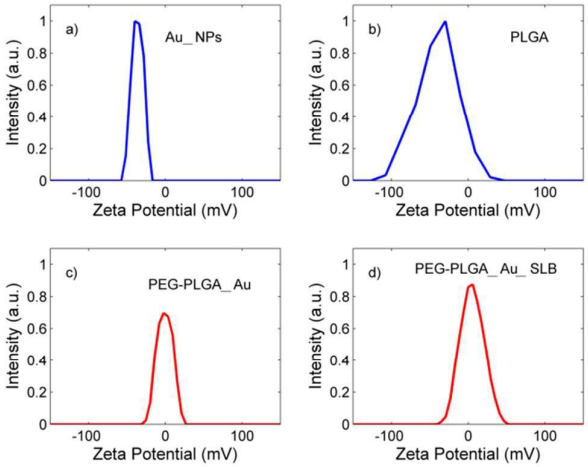

Fig. 10: Zeta potential values estimated by DLS.

3.2. Drug loading and release

Drug loading was determined by dissolving the lyophilized nanocomposite incorporating SLB in PBS, followed by sonication and centrifugation. After centrifugal removal of free SLB, the drug concentration in the system was determined spectrophotometrically by looking at the intensity of the characteristic feature located at 286 nm and denoted as λ_{max}. On the basis of optical absorbance data and molar extinction coefficient ($\varepsilon_{286} \cong 11320$ $M^{-1}cm^{-1}$), SLB loading in the nanocomposite was 0.088 mg of drug/mg of drug carrier. Thus we estimated that the drug loading efficiency is about 89% and the drug content is about 8.8%.

Generally, the polymeric nano-delivery systems containing stimuli-sensitive components are engineered to be activated, on demand, for a spatial-temporal and dosage-controlled release of drugs at the site of interest. While the internal stimuli are dependent on the characteristics of the biological systems, electromagnetic waves (visible/near-infrared light) are independent of the biological environment and can be actively and externally manipulated. Sometimes the low energy of the diode laser light in the near-infrared spectral region could be not sufficient to directly initiate the cleavage of chemical bonds often required for releasing the drugs. To overcome these limitations, approaches using heat-sensitive smart polymer composites, stimulated by visible higher power (80 mW) laser light are adopted.[65] However, the drug release activation by high power visible laser light could have, as a negative effect, the partial tear of human tissue.

Thus, we propose herein to activate our nano-SLB delivery system with a red laser source of relatively low power density (21 mW/cm^2), partially transparent to human flesh. Firstly, a 532 nm laser was adopted but immediately discarded since both the SLB and the PEG-PLGA copolymer resulted unstable.

With the aim to explore a protocol for therapeutic treatments which require a fast pharmacological action, drug release was monitored only for a short time dynamics, using the dialysis bag technique. Thus, the PEG-PLGA_Au-SLB nanocomposite was suspended in PBS (pH 7.4) at 37°C and the release of the drug was studied for 3 days. Fig. 11 shows the relative release increment observed for the irradiated sample with respect to the not irradiated one, as a function of the time. It is evident that in the first 5 h the drug release increment is about 75%, while it is nearly halved over 20 h, and remains almost unchanged for even longer times. This behavior can be explained taking into account the morphology of the nanocomposite and the distribution of the Au NPs and the SLB within the polymeric system. The initial SLB release (within the 5h) from the spherical polymeric structures is due to the diffusion of the drug from the 200 nm sized particles. This mechanism is aided by the Au-mediated laser irradiation heating effect, making more effective the diffusion process, so that a higher percentage of SLB is released upon irradiation within a few hours with respect to the not irradiated sample.

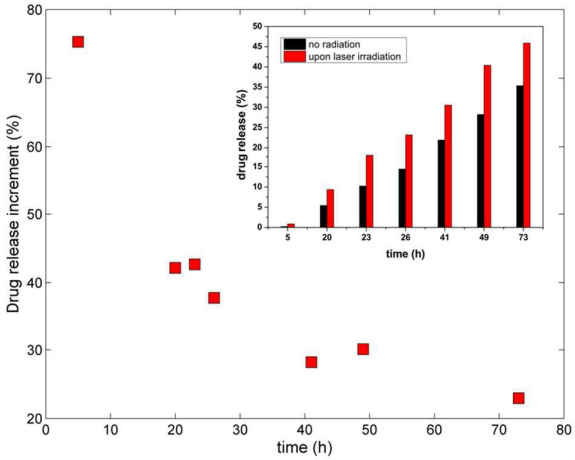

Fig. 11: Percentage incremental release of SLB from the PEG-PLGA_Au nanosystem irradiated by a 632.8 nm laser light source. In the inset, the cumulative release as a function of the time is reported.

According to a diffusion model and under the assumptions of a homogenous drug distribution,[66] the estimated value of SLB diffusivity for 200 nm sized PEG-PLGA particles under irradiation is 9.1×10^{-17} cm^2/s, which is nearly two order of magnitude higher with respect to the not irradiated sample

(for details about the diffusivity value determination, see SI). These values are almost comparable with the diffusivity values reported in literature for other polymeric systems encapsulating drugs,[67,68] taking into account the difference in polymer molecular weight, the presence of PEG chains and possible thermally-induced changes and/or degradation in the polymer morphology.[69]

No initial burst effect has been observed, indicating that the drug is, more likely, not weakly adsorbed onto the surface. Moreover, according to literature data,[59,70] the overall slow release kinetics of SLB (see the inset of Fig. 11, where the cumulative release, defined as the percentage ratio of released SLB to total loaded SLB is reported) is related to a strong interaction of the drug with the composite, due to the hydrophobic nature of SLB, and it suggests homogeneous entrapment of the drug throughout the system. Indeed, when the drug is uniformly dispersed within the matrix, the release occurs by a combination of drug diffusion, polymer swelling/degradation, erosion of the matrix.[71,72] These processes are responsible for the slow drug release, with a relevant contribution of the Au NPs that, under laser light irradiation, significantly improved the SLB release rate. Finally, the effects of irradiation on SLB were spectrometrically examined, resulting that the drug was not affected by the laser light.

Conclusions

The synthesis and characterization of a new water dispersible PEGylated-PLGA gold nanocomposite are presented. The ternary nanocomposite owns multifunctional properties, such as optical and hyperthermic/photothermal ones, which make it an interesting material for biomedical applications. The ability of the nanoplatform to encapsulate and to release SLB, working as a controlled light-triggered DDS, has been investigated. Indeed, the results show that the drug is released more effectively upon light irradiation in an active and time definite way. In particular, the SLB release increment reaches 75% within the first 5 hours, and it lowers to a 30% (or lower) value within 48 hours.

Then, by encapsulating appropriate drugs, the proposed nanovector could be used for photothermal therapies that make use of visible optical radiation due to the presence of Au NPs. In principle and taking into account of the novelty from the fiber-fabrication technology, an injector including an optical fiber could be engineered to administer and deliver the light radiation to the tumor.

Technological advances may suggest the use of more sophisticated wirelessly controlled nanowires responding to an electromagnetic field generated by a separate device. This engineering system eliminates tubes and wires required by other implantable devices that can lead to infections and other complications, whilst activating drug release in proximity of areas of the body that are often difficult to access.

Acknowledgements

This work was partially funded by the European Community through the Programma Operativo Nazionale Ricerca e Competitività 2007−2013 (PON02_00355_2964193 Hippocrates Project).

Notes and references

1 F. D. Jochumab, P. Theato, *Chem. Soc. Rev.,* 2013, **42**, 7468.
2 R. Tong, L. Tang, L. Ma, C. Tu, R. Baumgartnerb, J. Cheng *Chem. Soc. Rev.*, 2014, **43**, 6982.
3 K. Rahme, M. T. Nolan, T. Doody, G. P. McGlacken, M. A. Morris, C. O'Driscolle, J. D. Holmes, *RSC Adv.*, 2013, **3**, 21016 and references cited therein.
4 J. Geng , K. Li , K. Y. Pu , D. Ding, B. Liu, *Small*, 2012, **8**, 2421 and references cited therein.
5 K. Rahme, L. Chen, R. G. Hobbs, M. A. Morris, C. O'Driscolle, J. D. Holmesab, *RSC Adv.*, 2013, **3**, 6085 and references cited therein.
6 K. Niikura, N. Iyo, Y. Matsuo, H. Mitomo, K. Ijiro *ACS Appl. Mater. Interf.,* 2013, **5**, 3900.
7 L. Paasonen, T. Laaksonen, C. Johans, M. Yliperttula, K. Kontturi, A. Urtti, *J. Control. Release,* 2007, **122**, 86.
8 A. S. Angelatos, B. Radt, F. Caruso, *J. Phys. Chem. B,* 2005, **109**, 3071.
9 Y. Wang, B. Li, L. Zhang, H. Song, L. Zhang, *ACS Appl. Mater. Interf.,* 2013, **5**, 11.
10 M. Bikram, A. M. Gobin, R. E. Whitmire, J. L. West, *J. Control. Release,* 2007, **123**, 219.
11 M. M. Kemp, A. Kumar, S. Mousa, T. J. Park, P. Ajayan, N. Kubotera, S. A. Mousa, R. J. Linhardt, *Biomacromolecules*, 2009, **9**, 589 and references cited therein.
12 L. Juillerat-Jeanneret, *Drug Discov Today*, 2008, **13**, 1099.
13 J. Manson, D. Kumar, B. J. Meenan, D. Dixon, *Gold Bull*, 2011, **44**, 99.
14 S. Chen, K. Kimura, *Langmuir*, 1999, **15**, 1075.
15 L. Lascialfari, P. Marsili, S. Caporali, M. Muniz-Miranda, G. Margheri, A. Serafini, A. Brandi, E. Giorgetti, S. Cicchi, *Thin Solid Films*, 2014, **569**, 93 and references cited therein.
16 J. P.Sylvestre, S. Poulin, A. V. Kabashin, E.Sacher, M. Meunier, J. H. T. Luong, *J. Phys. Chem. B*, 2004, **108**, 16864.
17 W. Qian, M. Murakami, Y. Ichikawa, Y.Che, *J. Phys. Chem. C*, 2011, **115**, 23293.
18 R. H.Prabhu, V. B. Patravale, M. D. Joshi, *Int. J. Nanomed.*, 2015, **10**, 1.
19 R. Gref, Y. Minamitake, M.T. Peracchia, V. Trubetskoy, V. Torchilin, R. Langer, *Science*, 1994, **263**, 1600.
20 S.B. La, T. Okano, K. Kataoka, *J. Pharm. Sci.*, 1996, **85**, 85.
21 G. S. Kwon, M. Yokoyama, T. Okano, Y. Sakurai, K. Kataoka, *Pharm Res*, 1993, **10**, 970.
22 H. S. Yoo, T. G. Park*, J. Control. Release*, 2001, **70**, 63.
23 H. Sah, L. A. Thoma, H.R. Desu, E. Sah, G. C. Wood, *Int. J. Nanomed.*, 2013, **8**, 747.
24 N. Kamalya, Z. Xiaoa, P. M. Valencia, A. F. Radovic-Moreno, O. C. Farokhzad, *ChemSoc Rev.*, 2012, **41(7)**, 2971.
25 For a recent review see: K. Zhang, X. Tang, J. Zhang, W. Lu, X. Lin, Y. Zhang, B. Tian, H.Yang, H. He, *J. Control. Release*, 2014, **183**, 77.
26 P. Gentile, V. Chiono, I. Carmagnola, P. V. Hatton, *Int. J. Mol. Sci.*, 2014, **15**, 3640.
27 D. T. T. Le, L. T. M. Dang, N. T. M. Hoang, H. T. La, H. T. M. Nguyen, H. Q. Le, *J Nanomed Nanotechnol*, 2015, **6**, 1000267.
28 E. Locatelli, M. C. Franchini, *J Nanoparticle Research*, 2012, **14**, 1316.

29 J. M. Chan, P. M. Valencia, L. Zhang, R. Langer, O. C. Farokhzad, *Methods in molecular biology*, 2010, **624,** 163.
30 J. Cheng, B. A. Teply, I. Sherifi, J. Sung, G. Luther, F. X. Gu, E. Levy-Nissenbaum, A F. Radovic-Moreno, R.Langer, O C. Farokhzad, *Biomaterials*, 2007,**28**, 869.
31 H. Wang, Y. Zhao, Y. Wu, Y-L. Hu, K. Nan, G. Nie, H. Chen, *Biomaterials*, 2011,**32**, 8281.
32 R. Kumar, A. Kulkarni, J. Nabulsi, D. K. Nagesha, R. Cormack, M. G. Makrigiorgos, S. Sridhar,*Drug DelivTransl*Res, 2013,**3(4)**, 299.
33 P.Zhao, H. Wang, M. Yu, Z. Liao, X. Wang, F.Zhang, W. Ji, B. Wu, J. Han, H. Zhang, H. Wang, J. Chang, R. Niu,*Eur J Pharmaceutics and Biopharmaceutics*, 2012, **81**, 248.
34 S. HS. Boddu, R. Vaishya, J. Jwala, A. Vadlapudi, D. Pal, A.K. Mitra,*Med chem*, 2012, **2(4)**, 068.
35 Z. Zhang, L.S. Huey, S.S. Feng, *Biomaterials*,2007, **28**, 1889.
36 K. Hu, J. Li, Y. Shen, W. Lu, X. Gao, Q. Zhang, X. Jiang, *J. Control. Release*, 2009, **134**,55.
37 V. Sanna, N. Pala, M. Sechi, *Int J Nanomed*, 2014, **9**, 467.
38 J. Hrkach, D. Von Hoff, Ali M.Mukkaram, et al.,*SciTransl Med.*, 2012, **4(128)**, 128.
39 C-H. Chu, Y-C. Wang, L-A. Tai, L-C. Wu, C-S. Yang, *J. Mat. Chem. B*, 2010, **20**, 3260.
40 M. Gajendiran, S. M. J. Yousuf, V. Elangovan, S. Balasubramanian, *J. Mat. Chem. B,* 2014, **2**, 418.
41 M. S. Yavuz, Y. Cheng, J. Chen, C. M. Cobley, Q. Zhang, M. Rycenga, J. Xie, C. Kim, A. G. Schwartz, L. V. Wang, Y. Xia, *Nat Mater*, 2009, **8(12)**, 935.
42 J. Yang, J. Lee, J. Kang, S. J. Oh, H.-J. Ko, J.-H. Son, K. Lee, J.-S. Suh, Y.-M. Huh, S. Haam, *Adv Mater*, 2009, **21**, 4339.
43 C.-H. Chu, Y.-C. Wang, L.-A. Tai, L.-C. Wu, C.-S. Yang,*J. Mater. Chem.*, 2010, **20**, 3260.
44 K.Niikura, N. Iyo, Y. Matsuo, H. Mitomo, K. Ijiro,*ACS Appl. Mater. Interfaces*, 2013, **5**, 3900.
45 J.F.Liao, W.T. Li, J.R. Peng, Q. Yang, H. Li, Y.Q. Wei, X.N. Zhang, Z.Y. Qian, *Theranostic*, 2015,**5(4)**, 345.
46 X. Wu, Y. Gao, C.-M. Dong, *RSC Adv*, 2015, **5**, 13787.
47 D. Dixon B. J. Meenan, J. Manson, *J NanoResearch*, 2014, **27**, 83.
48 S.-M. Lee, H. J. Kim, Y.-J. Ha, Y. N. Park, S.-K. Lee, Y.-B. Park, K.-H. Yoo, *ACS Nano*, 2013, **7**, 50.
49 S.-M. Lee, H. Park , K.-H. Yoo, *Adv Mater*, 2010, **22**, 4049.
50 M. Gajendiran, S. M. J. Yousuf, V. Elangovan, S. Balasubramanian, *J Mat Chem B*, 2014, **2**, 418.
51 C.V. Kavitha , G. Deep, S.C. Gangar, A.K. Jain, C. Agarwal, R. Agarwal, *Mol Carcinog.,* 2014, **53**, 169.
52 G-J. Cui, L-M. Xu, Y. Zhou, J-J. Zhang, J-X. Wang, J-F. Chen, *Chem. Eng. J.*, 2013 **222**, 512.
53 L. Jia, D. Zhang, Z. Li, C. Duan, Y. Wang, F. Feng, F. Wang, Y. Liu, Q. Zhang, *Colloids Surf. B: Biointerfaces,* 2010, **80**, 213.
54 P. Xu, Q. Yin, J. Shen, L. Chen, H. Yu, Z. Zhang, Y. Li, *Int. J. Pharm.* 2013, **454**, 21.
55 J. Q. Zhang, J. Liu, X. L. Li, B. R. Jasti, *Drug Delivery*, 2007, **14**, 381.
56 J-K. Cho, J. W. Park, S-C. Song, *J. Pharm. Sci.*, 2012, **101**, 2382.
57 Y. Wei, X. Ye, X. Shang, X. Peng, Q. Bao, M. Liu, M. Guo, F. Li, *Colloids Surf. A: Physicochem. Eng. Aspects,* 2012, **396**, 22.
58 D. H. Kim, M. D. Kim, C. W. Choi, C. W. Chung, S. H. Ha, C. H. Kim, Y. H. Shim, Y. I. Jeong, D. H. Kang, *Nanoscale Research Letters*, 2012, **7**, 91.
59 Y-Il Jeong, D. H. Kim, C-W. Chung, J-J. Yoo, K. H. Choi, C. H. Kim, S. H. Ha, D. H. Kang, *Int. J. Nanomed.*, 2011, **6**, 1415.
60 T. Kitayama, K. Hatada, in NMR Spectroscopy of Polymers, ed. Roger N. Ibbett, Springer–Verlag Berlin Heidelberg, New Jork 2004, ch. 4.
61 Scofield, J. H. Hartree, *J. Electron Spectrosc. Relat. Phenom.*,1976, **8**, 129.
62 E. Pisani, C. Ringard, V. Nicolas, E. Raphael, V. Rosilio, L. Moine, E. Fattal, N. Tsapis, *Soft Matter,* 2009, **5**, 3054.
63 S. Näkki, J. Rytkönen, T. Nissinen, C. Florea, J. Riikonen, P. Ek, H. Zhang, H.A. Santos, A. Närvänen, W. Xu, V.P. Lehto, *Acta Biomater.,* 2015, **13**, 207.
64 P. Zhao, H. Wang, M. Yu, Z. Liao, X. Wang, F. Zhang, W. Ji, B. Wu, J. Han, H. Zhang, H. Wang, J. Chang, R. Niu, *Eur. J. Pharm. Biopharm*, 2012, **81,** 248.
65 S. J. Leung, M. Romanowski, *Theranostics.* 2012; **2**, 1020.
66 J. Siepmann, N.A. Peppas, Advanced Drug Delivery Reviews 2001, 48, 139.
67 A. Budhian, S. J. Siegel, K. I. Winey, *Int. J. of Pharm.*, 2008, **346,** 151.
68 T.R. Tice, S.E. Tabibi, Parental Drug Delivery: Injectable, in A. Kydonieus (Ed.), Treatise on controlled drug delivery, Marcel Dekker, Inc. New York, 1992, pp. 315-339
69 A. P. Esser-Kahn, S. A. Odom, N. R. Sottos, S.R. White, J. S. Moore, *Macromolecules*, 2011, **44**, 5539.
70 R. Paliwal, S. Rai, B. Vaidya, K. Khatri, A. K. Goyal, N. Mishra, A. Mehta, S. P. Vyas, *Nanomed. Nanotechnol.*, 2009, **5**, 184.
71 M. Stevanovic, D. Uskokovic, *Current Nanoscience*, 2009, **5**, 1.
72 H. K. Makadia, S. J. Siegel, *Polymers*, 2011, **3**, 1377.